NANO LETTERS

Letter

pubs.acs.org/NanoLett

Ultrafast Supercontinuum Spectroscopy of Carrier Multiplication and Biexcitonic Effects in Excited States of PbS Quantum Dots

F. Gesuele,*[,†] M. Y. Sfeir,[‡] W.-K. Koh,[§] C. B. Murray,[§,∥] T. F. Heinz,[⊥] and C. W. Wong*[,†]

[†]Optical Nanostructures Laboratory, Center for Integrated Science and Engineering, Solid-State Science and Engineering, and Mechanical Engineering, Columbia University, New York, New York 10027, United States

[‡]Center for Functional Nanomaterials, Brookhaven National Laboratory, Upton, New York 11973, United States

[§]Department of Chemistry and [∥]Department of Materials Science and Engineering, University of Pennsylvania, Philadelphia, Pennsylvania 19104, United States

[⊥]Departments of Physics and Electrical Engineering, Columbia University, New York, New York 10027, United States

ABSTRACT: We examine the population dynamics of multiple excitons in PbS quantum dots using spectrally resolved ultrafast supercontinuum transient absorption (SC-TA) measurements. We simultaneously probe the first three excitonic transitions. The transient spectra show the presence of bleaching of absorption for the $1S_h-1S_e$ transition, as well as transients associated with the $1P_h-1P_e$ transition. We examine signatures of carrier multiplication (multiple excitons arising from a single absorbed photon) from analysis of the bleaching features in the limit of low absorbed photon numbers ($\langle N_{abs}\rangle \sim 10^{-2}$) for pump photon energies from two to four times that of the band gap. The efficiency of multiple-exciton generation is discussed both in terms of the ratio between early- to long-time transient absorption signals and of a broadband global fit to the data. Analysis of the population dynamics shows that bleaching associated with biexciton population is red shifted with respect to the single exciton feature, which is in accordance with a positive binding energy for the biexciton.

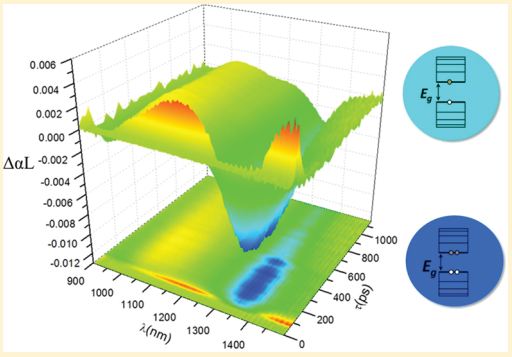

KEYWORDS: *Multiple-exciton generation, carrier multiplication, solar cells, ultrafast spectroscopy*

There is great interest in the properties of quantum dot (QD) based-materials for third-generation photovoltaics.[1,2] The strong spatial confinement of electronic wave function has been evoked as a route toward enhancements of carrier−carrier interactions. Further, the existence of separated, quantized energy levels may act to reduce the rate of phonon emission from highly excited carriers. It has been argued that these effects can contribute to the efficiency of carrier multiplication (CM) or multiple-exciton generation (MEG), the processes in which absorption of a single high-energy photon leads to the production of more than one electron−hole pair.[3,4] In addition to spatially separated multiple excitons,[5] this effect is a promising mechanism to enhance the solar cell efficiency, by means of an increase in the photocurrent,[6] beyond the classic Shockley−Queisser limit.[7]

In recent years, evidence of carrier multiplication has been reported, but the results appear to depend strongly on sample preparation, experimental conditions, and the detailed interpretation of the measurements.[8−16] Although recent studies[17,18] in chemically synthetized materials indicate the existence of enhanced photocurrent from carrier multiplication, there has been considerable uncertainty about the precise efficiency of this process and, accordingly, its possible impact on practical photovoltaic devices. To date, most studies of CM in quantum dots have been carried out by following the carrier dynamics through purely optical measurements. Techniques that have been applied include terahertz pump−probe spectroscopy[19,20] and time-resolved photoluminescence measurements.[21,22] The majority of the investigations have, however, relied on transient measurements of changes in the interband absorption induced by an ultrafast pump pulse.[23,24] These studies have focused on the lowest energy, $1S_h-1S_e$, absorption feature and have generally involved detection of the transient absorption at one or a few discrete wavelengths.[10,12,27,28] So far the results have not explicitly taken into account the homogeneous and ensemble broadening of first exciton peak, which is ∼100 meV at room temperature.[25,26]

In this Letter, we investigate the multiple-exciton generation and dynamics in PbS QDs by means of ultrafast supercontinuum transient absorption (SC-TA) spectroscopy. Our measurements simultaneously probe the spectral region defined by first three excitonic interband transitions ($1S_h-1S_e$, $1P_h-1P_e$, and $1S_{h,e}-1P_{h,e}$). We examine the dynamics induced by photoexcitation of the QDs at pump photon energies from two to four times the band gap. Observation of the spectrally

Received: June 23, 2011
Revised: November 17, 2011
Published: December 8, 2011

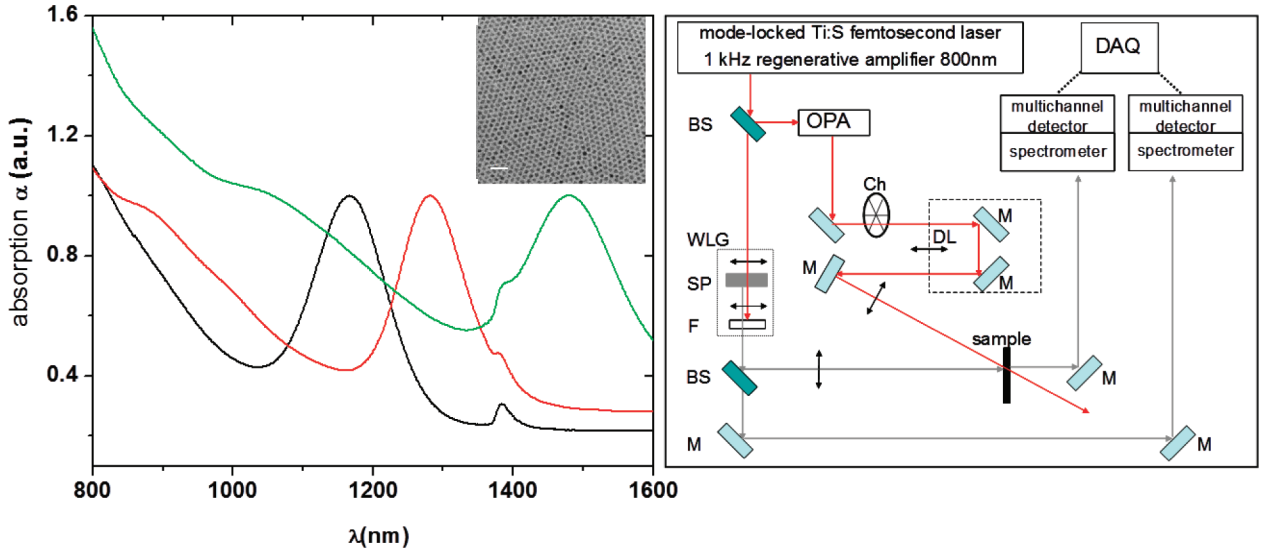

Figure 1. PbS nanocrystals for multiple exciton generation and ultrafast dynamics studies. (Left) Linear absorption spectra for nanocrystals of varying diameter. The absorption feature near 1400 nm arises from the fused quartz cuvette and does not affect the time-resolved data Inset: High-resolution transmission electron microscopy image of the PbS nanocrystals. Scale bar: 10 nm. (Right) Schematic representation of the instrument for ultrafast supercontinuum transient absorption spectroscopy. The system is based on an amplified 800 nm modelocked Ti:sapphire laser and a pair of multichannel optical detectors for the spectrally dispersed light. Other components include an OPA, optical parametric amplifier; DL, delay line; M, mirror; BS, beam splitter; WLG, white-light generator; SP, sapphire plate; DAQ, high-speed data acquisition; Ch, optical chopper; F, color filter.

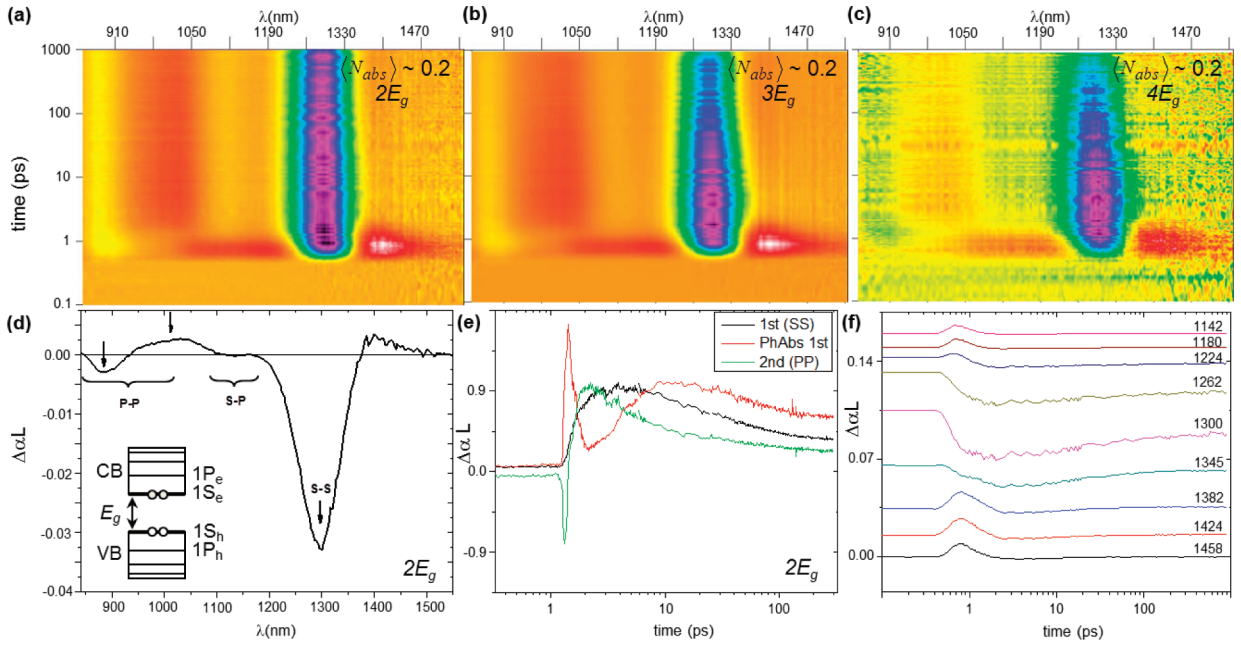

Figure 2. Transient absorption spectra for PbS nanocrystals with the first exciton transition at 1310 nm. (a–c) SC-TA spectra for pump excitation at wavelengths of 640 nm ($2E_g$), 427 nm ($3E_g$) and 320 nm ($4E_g$), respectively. The pump fluence was adjusted to yield $\langle N_{abs} \rangle \sim 0.2$ for the three cases. (d) The differential absorption spectrum at a delay time of 1.5 ps. The data were obtained for excitation at 640 nm at a pump fluence leading to $\langle N_{abs} \rangle \sim 1.3$. Note the presence of two bleach bands, near the first and second exciton transitions, as well as a region of photoinduced absorption. The spectral region with little induced change is associated with the 1PA forbidden S–P transition. (e) Dynamics of first and second bleaches (sign-inverted) and of the photoinduced absorption band under the same conditions as in (d). The wavelengths of the spectra correspond to the arrows in panel (d), and the vertical scales of the curves have been adjusted for clarity. (f) Representative bleach dynamics measured at different wavelengths, as indicated on each trace, near the first exciton peak (1310 nm). The data were obtained for excitation at 640 nm at a pump fluence leading to $\langle N_{abs} \rangle \sim 1$.

resolved ultrafast dynamics enables us characterize the response associated with the different transitions and, importantly, to perform a global analysis of the carrier dynamics.

The samples investigated in this work were oleic-acid-capped PbS QDs. The nanocrystals were synthesized in an oxygen-free glovebox[29] and suspended in trichloroethylene (TCE) for study. The samples were rapidly transferred, while still inside the glovebox, to fused quartz cuvettes filled with the solvent and subsequently sealed to prevent oxygen exposure during the course of our studies. Optical absorption spectra, shown in

dx.doi.org/10.1021/nl2021224 | Nano Lett. 2012, 12, 2658–2664

Figure 1a, were obtained over the spectral range of supercontinuum probe (800−1600 nm). The narrow size distribution of QD samples allows the ready identification of the optical absorption features. The data clearly show two well-defined absorption peaks at the spectral positions reported in the literature.[30,31] The lower-energy feature arises from the $1S_h-1S_e$ transition; the identification of the second peak in PbS QDs has been the subject of some recent debate.[30,32−34]

Following the energy-level calculation presented in literature based on the four-band k·p envelope model[35] including band[36] or wave function anisotropy,[30] we attribute the second peak to the (one-photon) allowed $1P_h-1P_e$ transition.[37] Part of the finite absorption in the region between this peaks, particularly near the minimum absorption, may be associated with the nominally forbidden one-photon absorption (1PA) from $1S_{h,e}-1P_{h,e}$ transitions.[33] Within a purely isotropic model, we expect no 1PA transitions among the S and P levels because of the wave function parity. Recent work[30] has, however, pointed out that symmetry breaking in the wave function can explain the 1PA from $1S_{h,e}-1P_{h,e}$ transitions (as well as two-photon absorption for the $1S_h-1S_e$ and $1P_h-1P_e$ transitions).

The experiments made use of a 1 mJ Ti:sapphire femtosecond regenerative amplifier operating at a repetition rate of 1 kHz. Combined with an optical parametric amplifier (OPA), this system generates sub-100 fs pulses in the ultraviolet, visible, and infrared spectral regions (Newport Spectra-Physics). This source, illustrated in Figure 1b, is coupled to a supercontinuum transient absorption spectrometer, which provides approximately 100 fs temporal resolution over a time window up to 3 ns. The detection consists of a pair of high-resolution (512 pixel) multichannel detector arrays coupled to a high-speed data acquisition system (Ultrafast Systems). In our measurements, the samples are optically pumped using the spectrally tunable (240 to 2600 nm) femtosecond pulses generated in the OPA. The induced changes in transmission are probed using the white-light supercontinuum radiation over a range of wavelengths from 850−1600 nm. We note that the probe power over the entire spectrum is only a few hundred nanowatts. It is well below that of the pump, even for measurements made at low pump powers, and can be considered as nonperturbative.

During the experiments, the samples were vigorously stirred in the trichloroethylene solution to avoid laser-induced modification of the nanocrystals. The circulation of the QDs strongly reduces pump-induced modification of the samples, such as photoionization, which can lead to the presence of additional rapid decay channels that complicate analysis of multiple-exciton generation.[38] Also, to avoid artifacts from direct generation of multiple excitations by the absorption of more than one photon, the number of absorbed photons $\langle N_{abs}\rangle$ was carefully controlled as an important experimental parameter. Its value is estimated using the experimental pump pulse fluence J (photons/cm^2) and the QD absorption cross-section σ_a at the relevant pump wavelength by $\langle N_{abs}\rangle = J\,\sigma_a$.[39,31,40]

Figure 2a−c displays typical spectrally resolved differential absorption for a QD sample with its first exciton absorption peak centered at 1310 nm. The two-dimensional (2D) time-resolved spectrograms cover the energy of the first three excitonic transitions, as discussed above, over a time window of 1 ns. These time and spectrally resolved measurements were corrected for the chirp of the broadband probe pulse, which was measured independently under the same experimental condition using neat solvent in place of nanocrystal solution. Such spectrally resolved pump−probe measurements were performed with excitation photon energies of 2, 3, and 4 times the QD gap energy. The pump fluence was adjusted to remain within the limit of low excitation density, maintaining the same estimated number of absorbed photons per QD for the three sets of data ($\langle N_{abs}\rangle \sim 0.2$).

Figure 2d is a differential absorption spectrum obtained at a fixed delay time of 1.5 ps. We can clearly identify two spectral bands of bleaches. The first one corresponds to the fundamental exciton transition observed in linear absorption. At shorter wavelength, we then see a region with relatively little induced change in absorption, even at high pump fluence. We ascribe this behavior to the spectral region of the 1PA forbidden $1S_{h,e}-1P_{h,e}$ transition. At still shorter wavelengths, we observe a photoinduced absorption band, followed by the second bleach band. We attribute both the photoinduced absorption and the second bleach band primarily to the role of the transition $1P_h-1P_e$. The observed behavior can be understood not predominantly as a population effect, but rather as reflecting a red shift of the $1P_h-1P_e$ transition associated with the presence of the $1S_h-1S_e$ excitons created by the pump pulse.[31,38] The positive band displays an asymmetric line shape, presumably indicating the superposition of pure electron and pure hole intraband transitions or of excited-state absorption.

In Figure 2e, we plot the (normalized) time evolution of the $1S_h-1S_e$ and$1P_h-1P_e$ bleaches, as well as of the photoinduced absorption band. The data were obtained for excitation at $2E_g$, but at high fluence ($\langle N_{abs}\rangle \sim 1.3$). Under these conditions, no CM is expected, but some multiple excitons are generated directly by the absorption of more than one photon in a given QD. Compared with the first ($1S_h-1S_e$) bleach band, we observe that the second ($1P_h-1P_e$) bleach exhibits a somewhat faster decay and a minimum at earlier time. This behavior can be understood if the relaxation processes from the high-lying excitonic states occur on the time scale of a few hundred femtoseconds. Assuming essentially instantaneous pumping compared to the time resolution of our supercontinuum probe, the initial rise of second transition bleach to its maximum corresponds to relaxation from higher-lying states to $1P_h-1P_e$. The time interval between the maximum of the first and second bleaches corresponds to relaxation from $1P_h-1P_e$ to $1S_h-1S_e$ states. The slower decay component with comparable time constants for each of the three cases suggests that Auger recombination processes involve not only the first but also the second bleach. This is reasonable considering that the exciton generation and recombination is a process that couples these bands since it simultaneously changes the electron and hole occupation numbers. When Auger recombination occurs, the energy of one exciton goes into excitation of an electron and/or hole to a higher-lying state from which it will relax through the intermediate excited states. In Figure 2f, we illustrate the variation of the dynamics as a function of probe wavelength around the first transition. The spectral variation of initial rise and of the photoinduced absorption can be seen in the early time dynamics, which is in accord with previous observations.[10] The positive transient at longer-wavelengths has been attributed to excited state absorption.[47]

The efficiency of multiple-exciton generation process can be estimated using the observation[23] of the Auger recombination of a biexciton in the lowest-lying $1S_h-1S_e$ state into a single high-energy exciton, which subsequently relaxes to yield a

dx.doi.org/10.1021/nl2021224 | Nano Lett. 2012, 12, 2658−2664

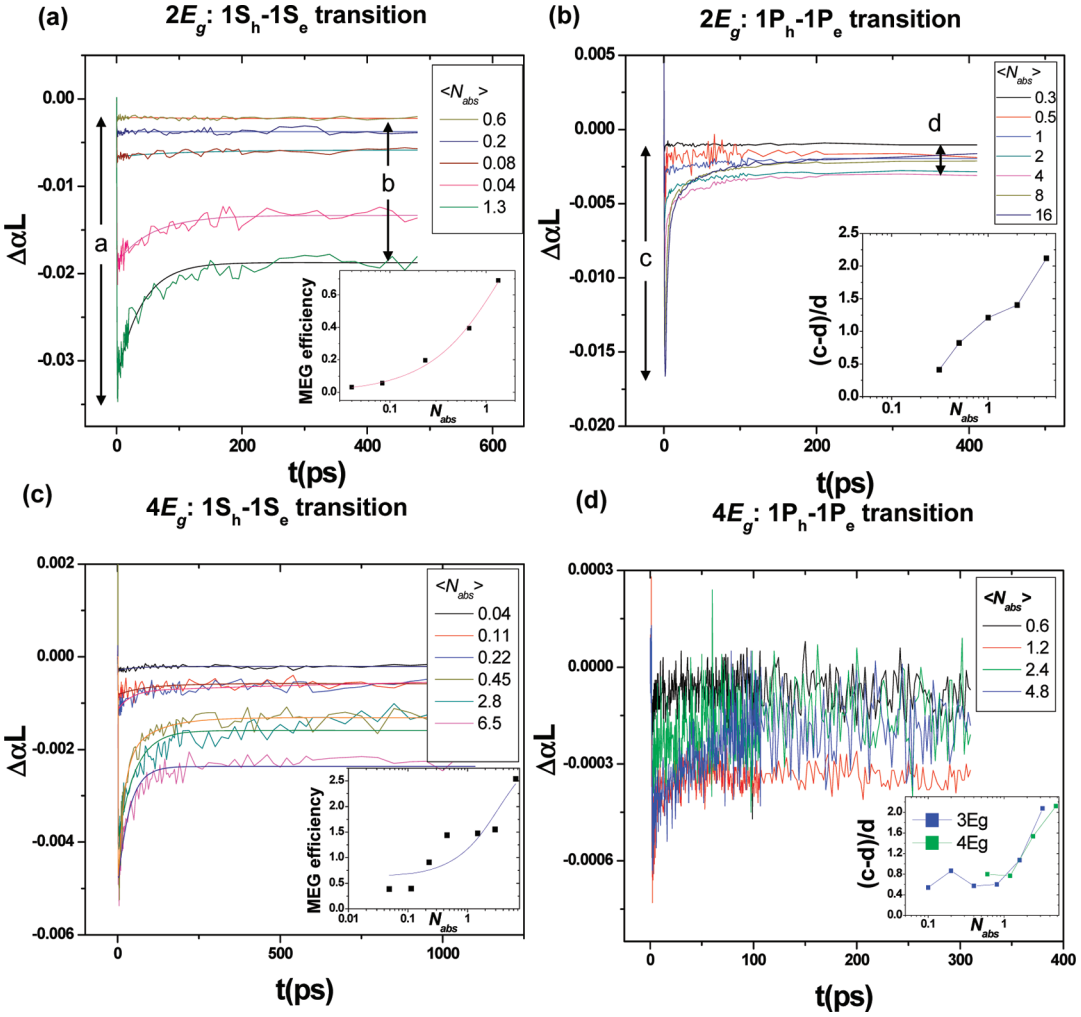

Figure 3. (a,c) Bleach dynamics for first excitonic transition for pump photon energies of $2E_g$ and $4E_g$, respectively. The inset shows the corresponding MEG efficiency, calculated from the ratio of early to late time response. A finite asymptotic value at low pump fluence indicates the presence of carrier multiplication. (b,d) Corresponding bleach dynamics for second excitonic transition for pump photon energies of $2E_g$ and $4E_g$, respectively. The inset shows the parameter for the inferred carrier multiplication based on $(c - d)/d$ for $2E_g$ (b), $3E_g$, and $4E_g$ (d).

single $1S_h{-}1S_e$ exciton. As seen in Figure 3, this process happens in tens of picoseconds. If we assume that the magnitude of the bleach is directly proportional to the exciton population, then the ratio of the maximum enhancement in the bleaching at early time $(a - b)$ to the long-time asymptotic value (b) of the bleaching yields the efficiency for multiple-exciton generation. This analysis assumes that the change in the transient absorption scales directly with the average number of excitons present. To avoid the complication of the multiple excitons generated by directly by multiphoton absorption, our SC-TA measurements were performed at very low pump fluence, down to the limit of $\langle N_{abs}\rangle \sim 0.01$.

In Figure 3, we present a series of transient absorption spectra for both the $1S_h{-}1S_e$ (a,c) and $1P_h{-}1P_e$ (b,d) bands for different pump fluences and pump photon energies of $2E_g$ (Figure 3a,b) and $4E_g$ (Figure 3c,d). The insets in Figures 3a,c summarize the inferred multiple-exciton generation efficiency $[(a - b)/b = a/b - 1 = R - 1]$ as a function of $\langle N_{abs}\rangle$ for the first transition bleach. We fit the behavior for higher values of pump fluence (and $\langle N_{abs}\rangle$) following the analysis of Beard et al.[2,23] based on a Poissonian distribution of absorbed photons.

The asymptotic behavior at low pump fluence ($\langle N_{abs}\rangle \sim 0.01$) directly yields the efficiency for multiple exciton generation. For pump excitation at $4E_g$, there is a clear signature of CM. No measurable CM is observed, however, for excitation at $2E_g$, with multiple excitons arising only from the absorption of multiple photons. Figures 3b,d present the corresponding pump-dependent bleaches for the $1P_h{-}1P_e$ transition for excitation at photon energies of $2E_g$ and $4E_g$. We show the maximum induced bleaching at early time $(c - d)$ and the long-time asymptotic value (d) for the $1P_h{-}1P_e$ transition. We observe that, in analogy to the $1S_h{-}1S_e$ dynamics, at low $\langle N_{abs}\rangle$ values the $1P_h{-}1P_e$ ratio $(c - d)/d$ at $4E_g$ asymptotes to a nonzero value, highlighting the presence of carrier multiplication; for excitation at $2E_g$, this ratio assumes an asymptotic value of zero, corresponding to the absence of carrier multiplication. The dynamics of this higher-order transition serves as an alternative approach to identify carrier multiplication. In absence of multiple excitons, the ratio tends to zero because the bleach is constant on the initial picosecond time scale.

To account for the spectral variation in the dynamics, we evaluate the broadband ultrafast dynamics with global fits via singular-value decomposition. In such an exponential regression analysis, we assume that the temporal evolution at each different wavelength is given by the same three lifetimes, but

dx.doi.org/10.1021/nl2021224 | Nano Lett. 2012, 12, 2658–2664

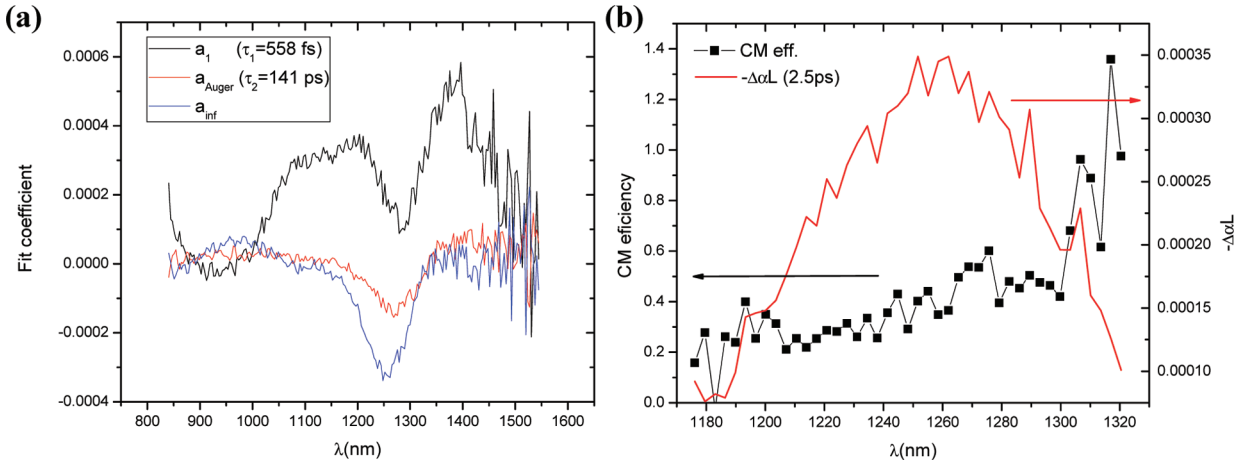

Figure 4. (a) Global fit coefficients for PbS nanocrystals pumped at $4E_g$ and $\langle N_{abs}\rangle \sim 0.04$. (b) The resultant spectrally resolved CM efficiency (black dotted) obtained from the ratio between a_{Auger} and a_∞. The differential absorption spectrum is superimposed (red line) for comparison.

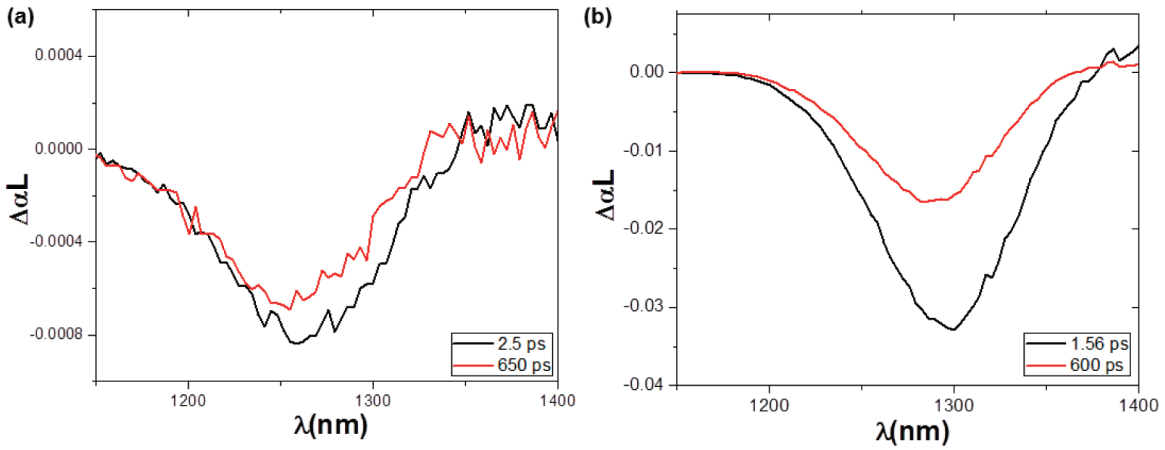

Figure 5. (a) Differential spectra at early (2.5 ps) and late times (650 ps), showing an early red shift from the presence of biexcitons. The pump photon energy was $4E_g$ and the excitation fluence yielded $\langle N_{abs}\rangle \sim 0.1$. (b) Same comparison for $2E_g$ and $\langle N_{abs}\rangle \sim 1.3$ also shows the biexciton shift.

with different weights. This corresponds to a description of the overall 2D measured differential absorption by

$$\Delta\alpha L(\lambda, t) = a_1(\lambda)\exp\left(-\frac{t-t_0}{t_1}\right) + a_{Auger}(\lambda)\exp\left(-\frac{t-t_0}{t_{Auger}}\right) + a_\infty(\lambda)\exp\left(-\frac{t-t_0}{t_\infty}\right)$$

The interpretation of the three relaxation components is as follows: the first (t_1), in the range of hundreds of femtoseconds, corresponds to relaxation from higher-order transitions; the second (t_{Auger}), in the range of tens of picoseconds, corresponds to the Auger recombination process; and the third (t_∞), in the range of hundreds of nanoseconds, corresponds relaxation of a single exciton, by radiative emission or other processes.[41] The coefficients of the fit represent the molar differential absorption of the species multiplied by their concentration in the solution. In this analysis, a_{Auger} and a_∞ correspond, respectively, to the relaxation of the biexciton and single exciton species.[42,43] In the limit of low $\langle N_{abs}\rangle$, the ratio a_{Auger}/a_∞ represents the spectrally resolved CM efficiency. It is worth noting that in first approximation this ratio a_{Auger}/a_∞ is equivalent to $(a - b)/b$. The advantage of global fit coefficients is that they allow one to readily identify single and biexciton bands.

In Figure 4, we plot the coefficients of our exponential regression for excitation at $4E_g$ and $\langle N_{abs}\rangle \sim 0.04$ with the inferred CM efficiency (black dotted) shown in panel b. We observe that it is not constant over the width of first $1S_h-1S_e$ band transition (superimposed as red line) but increased monotonically with wavelength. This can be understood considering that the minima for the coefficients a_{Auger} and a_∞ happen at different wavelengths with $(a_{Auger})_{min}$ red shifted. This indicates that the early time exciton population, which decays with a lifetime defined by a_{Auger}, is red shifted with respect to late time spectra. We observe from the global fitting procedure that the coefficients at 558 fs show a positive value for S−S transition (indicating increased bleaching), but a negative value for P−P (indicating increased absorption). This behavior can be linked to the decay from the P−P state to S−S state.

The physical explanation of this effect lies in the population of $1S_h-1S_e$ state. In Figure 5a, we compare the differential spectra for excitation at $4E_g$ (with the presence of CM) at the early time maximum (~2.5 ps) with that for late times (~650 ps). The early time spectrum is red-shifted with respect to the late time spectrum (after Auger recombination) by ~7 meV for this example. The same behavior is observed for excitation at $2E_g$ at high $\langle N_{abs}\rangle$ (Figure 5b). The presence of a second exciton in the nanocrystal introduces an attraction or repulsion

dx.doi.org/10.1021/nl2021224 | Nano Lett. 2012, 12, 2658−2664

with a corresponding positive or negative biexciton binding energy.[44] In these symmetric core nanocrystals, positive binding energy is expected[45,46] and, hence, the red-shifted bleach. To our knowledge, this is the first observation of the positive biexciton binding energy in PbS QDs through analysis of transient absorption spectra. The spectral variation of a_{Auger}/a_{∞} makes this quantity unfit for a correct estimation of the CM efficiency. Performing a spectral integration of coefficient over the absorption feature can solve this problem. An accurate determination of CM efficiency can be obtained, in the limit of low absorption photon number, from $\int \alpha_{Auger} d\lambda / \int \alpha_{\infty} d\lambda$.

In conclusion, we have studied the ultrafast dynamics of PbS QDs with spectrally resolved interband transient absorption measurements. We see dynamics associated with both the $1S_h-1S_e$ and $1P_h-1P_e$ excitonic states. The presence of carrier multiplication can be inferred from the transient spectra near the $1S_h-1S_e$ transition, but is also reflected in the dynamics measured near the $1P_h-1P_e$ transition. The role of spectral shifts in the time evolution of the response is addressed by means of global fits using the singular-value decomposition procedure. This method highlights the red shift of spectra at early times associated with the presence of biexcitons. This effect must be taken into account for an accurate determination of the carrier multiplication efficiency.

AUTHOR INFORMATION

Corresponding Author

*E-mail: (F.G.) fg2251@columbia.edu; (C.W.W.) cww2104@columbia.edu.

ACKNOWLEDGMENTS

The authors acknowledge discussions with Drs. Jonathan Schuller, Jonathan Owen, James Misewich, James Yardley, David Reichman, and Charles Black. This work was supported by the Center for Redefining Photovoltaic Efficiency through Molecule Scale Control, an Energy Frontier Research Center funded by Office of Basic Energy Sciences of the U.S. Department of Energy under Award DE-SC0001085. Sample preparation by C.B.M. and W.K.K. was supported by the National Science Foundation through Award DMS-0935165, with partial support through the Nano/Bio Interface Center (Award NSEC DMR-0832802). Research carried out in part at the Center for Functional Nanomaterials, Brookhaven National Laboratory, which is supported by the U.S. Department of Energy, Office of Basic Energy Sciences, under Contract No. DE-AC02−98CH10886.

REFERENCES

(1) Nozik, A. J. Nanoscience and Nanostructures for Photovoltaics and Solar Fuels. *Nano Lett.* **2010**, *10*, 2735.

(2) Beard, M. C.; Midgett, A. G.; Hanna, M. C.; Luther, J. M.; Hughes, B. K.; Nozik, A. J. Comparing Multiple Exciton Generation in Quantum Dots To Impact Ionization in Bulk Semiconductors: Implications for Enhancement of Solar Energy Conversion. *Nano Lett.* **2010**, *10*, 3019.

(3) Franceschetti, A.; An, J. M.; Zunger, A. Impact Ionization Can Explain Carrier Multiplication in PbSe Nanocrystals. *Nano Lett.* **2006**, *6*, 2191.

(4) Rabani, E.; Baer, R. Theory of multiexciton generation in semiconductor nanocrystals. *Chem. Phys. Lett.* **2010**, *496*, 227.

(5) Timmerman, D.; Izeddin, I.; Stallinga, P.; Yassievich, I. N.; Gregorkiewicz, T. Space-separated quantum cutting with Si nanocrystals for photovoltaic applications. *Nat. Photonics* **2008**, *2*, 105.

(6) Nozik, A. J. Exciton Multiplication and Relaxation dynamics in Nanocrystals: Applications to ultrahigh-Efficiency Solar Photon Conversion. *Inorg. Chem.* **2005**, *44*, 6893.

(7) Shockley, W.; Queisser, H. J. Detailed Balance Limit of Efficiency of p-n Junction Solar Cells. *J. Appl. Phys.* **1961**, *32*, 510.

(8) Shaller, R. D.; Klimov, V. I. High Efficient Carrier Multiplication in PbSe Nanocrystals: Implication for Solar Energy Conversion. *Phys. Rev. Lett.* **2004**, *32*, 186601.

(9) Schaller, R. D.; Agranovich, V. M.; Klimov, V. I. High-efficiency carrier multiplication through direct photogeneration of multi-exciton via virtual single-exciton states. *Nat. Phys.* **2005**, *1*, 189.

(10) Ellingson, R. J.; Beard, M. C.; Johnson, J. C.; Yu, P.; Micic, O. I.; Nozik, A. J.; Shabaev, A.; Efros, A. L. Highly Efficient Multiple Exciton Generation in Colloidal PbSe and PbS Nanocrystals. *Nano Lett.* **2005**, *5*, 865.

(11) Schaller, R. D.; Sykora, M.; Pietryga, J. M.; Klimov, V. I. Seven Excitons at a Cost of One: Redefining the Limits for Conversion Efficiency of Photons into Charge Carriers. *Nano Lett.* **2006**, *6*, 424−429.

(12) Trinh, M. T.; Houtepen, A. J.; Schins, J. M.; Hanrath, T.; Piris, J.; Knulst, W.; Goosens, A. P. L. M.; Siebbeles, L. D. A. In Spite of Recent Doubts Carrier Multiplication Does Occur in PbSe Nanocrystals. *Nano Lett.* **2008**, *8*, 1713.

(13) Schaller, R. D.; Sykora, M.; Jeong, S.; Klimov, V. I. High-Efficiency Carrier Multiplication and Ultrafast Charge Separation in Semiconductor Nanocrystals Studied via Time-Resolved Photoluminescence. *J. Phys. Chem. B* **2006**, *110*, 25332.

(14) Beard, M. C.; Midgett, A. G.; Law, M.; Semonin, O. E.; Ellingson, R. J.; Nozik, A. J. Variations in the Quantum Efficiency of Multiple Exciton Generation for a Series of Chemically Treated PbSe Nanocrystal Films. *Nano Lett.* **2009**, *9*, 836.

(15) Sykora, M.; Koposov, A. Y.; McGuire, J. A.; Schulze, R. K.; Tretiak, O.; Pietryga, J. M.; Klimov, V. I. Effect of Air Exposure on Surface Properties, Electronic Structure and Carrier Relaxation in PbSe Nanocrystals. *ACS Nano* **2010**, *4*, 2021.

(16) Luther, J. M.; Beard, M. C.; Song, Q.; Law, M.; Ellingson, R. J.; Nozik, A. J. Multiple Exciton Generation in Films of Electronically Coupled PbSe Quantum Dots. *Nano Lett.* **2007**, *7* (6), 1779−1784.

(17) Sukhovatkin, V.; Hinds, S.; Brzozowski, L.; Sargent, E. H. Colloidal quantum-dot photodetectors exploiting multiexciton generation. *Science* **2009**, *324*, 1542.

(18) Sambur, J. B.; Novet, T.; Parkinson, B. A. Multiple exciton collection in a sensitized photovoltaic system. *Science* **2010**, *330*, 63.

(19) Beard, M. C.; Turner, G. M.; Schmuttenmaer, C. A. Terahertz Spectroscopy. *J. Phys. Chem. B* **2002**, *106*, 7146−7159.

(20) Pijpers, J. J. H.; Ulbricht, R.; Tielrooij, K. J.; Osherov, A.; Golan, Y.; Delerue, C.; Allan, G.; Bonn, M. Assessment of carrier-multiplication efficiency in bulk PbSe and PbS. *Nat. Phys.* **2009**, *5*, 811−814.

(21) Nair, G.; Geyer, S. M.; Chang, L. Y.; Bawendi, M. G. Carrier multiplication yields in PbS and PbSe nanocrystals measured by transient photoluminescence. *Phys. Rev. B* **2008**, *78*, 125325.

(22) McGuire, J. A.; Joo, J.; Pietryga, J. M.; Schaller, R. D.; Klimov, V. I. New aspects of carrier multiplication in semiconductor nanocrystals. *Acc. Chem. Res.* **2008**, *41*, 1810.

(23) Beard, M. C.; Ellingson, R. J. Multiple exciton generation in semiconductor nanocrystals: Toward efficient solar energy conversion. *Laser Photon. Rev.* **2008**, *2* (5), 377−399.

(24) Klimov, V. I.; McBranch, D. W. Femtosecond high-sensitivity, chirp-free transient absorption spectroscopy using kilohertz lasers. *Opt. Lett.* **1998**, *23*, 277.

(25) Peterson, J. J.; Krauss, T. D. Fluorescence Spectroscopy of Single Lead Sulfide Quantum Dots. *Nano Lett.* **2006**, *6*, 510.

(26) Bose, R.; Gao, J.; Sun, F. W.; McMillan, J. F.; Williams, A. D.; Wong, C. W. Cryogenic spectroscopy of ultra-low density colloidal lead chalcogenide quantum dots on chip-scale optical cavities towards single quantum dot near-infrared cavity QED. *Opt. Express* **2009**, *17*, 22474.

(27) Ji, M.; Park, S.; Connor, S. T.; Mokari, T.; Cui, Y.; Gaffney, K. J. Efficient Multiple Exciton Generation Observed in Colloidal PbSe Quantum Dots with Temporally and Spectrally Resolved Intraband Excitation. *Nano Lett.* **2009**, *9*, 1217.
(28) Cho, B.; Peters, W. K.; Hill, R. J.; Courtney, T. L.; Jonas, D. M. Bulklike Hot Carrier Dynamics in Lead Sulfide Quantum Dots. *Nano Lett.* **2010**, *10*, 2498.
(29) Murray, C. B.; Sun, S.; Gaschler, W.; Doyle, H.; Betley, T. A.; Kagan, C. R. Colloidal synthesis of nanocrystals and nanocrystal superlattices. *IBM J. Res. Dev.* **2001**, *45*, 47.
(30) Nootz, G.; Padilha, L. A.; Olszak, P. D.; Webster, S.; Hagan, D. J.; Van Stryland, E. W.; Levina, L.; Sukhovatkin, V.; Brzozowski, L.; Sargent, E. H. Role of Symmetry Breaking on the Optical Transitions in Lead-Salt Quantum Dots. *Nano Lett.* **2010**, *10*, 3577.
(31) Cademartiri, L.; Montanari, E.; Calestani, G.; Migliori, A.; Guagliardi, A.; Ozin, G. A. Size-Dependent Extinction Coefficients of PbS Quantum Dots. *J. Am. Chem. Soc.* **2006**, *128*, 10337.
(32) Trinh, M. T.; Houtepen, A. J.; Schins, J. M.; Piris, J.; Siebbeles, L. D. A. Nature of the Second Optical Transition in PbSe Nanocrystals. *Nano Lett.* **2008**, *8*, 2112.
(33) Schins, J. M.; Trinh, M. T.; Houtepen, A. J.; Siebbeles, L. D. A. Probing formally forbidden optical transitions in PbSe nanocrystals by time- and energy-resolved transient absorption spectroscopy. *Phys. Rev. B* **2009**, *80*, 035323.
(34) Wehrenberg, B. L.; Wang, C.; Guyot-Sionnest, P. Interband and Intraband Optical Studies of PbSe Colloidal Quantum Dots. *J. Phys. Chem. B* **2002**, *106*, 10634.
(35) Kang, I.; Wise, F. W. Electronic structure and optical properties of PbS and PbSe quantum dots. *J. Opt. Soc. Am. B* **1997**, *14*, 1632.
(36) Andreev, A. D.; Lipovskii, A. A. Anisotropy-induced optical transitions in PbSe and PbS spherical quantum dots. *Phys. Rev. B* **1999**, *59*, 15402.
(37) Liljeroth, P.; Zeijlmans van Emmichoven, P. A.; Hickey, S. G.; Weller, H.; Grandidier, B.; Allan, G.; Vanmaekelbergh, D. Density of States Measured by Scanning-Tunneling Spectroscopy Sheds New Light on the Optical Transitions in PbSe Nanocrystals. *Phys. Rev. Lett.* **2005**, *95*, 086801.
(38) McGuire, J. A.; Sykora, M.; Joo, J.; Pietryga, J. M.; Klimov, V. I. Apparent Versus True Carrier Multiplication Yields in Semiconductor Nanocrystals. *Nano Lett.* **2010**, *10*, 2049.
(39) Klimov, V. I. Spectral and Dynamical properties of multiexcitons in semiconductor nanocrystals. *Annu. Rev. Phys. Chem.* **2007**, *58*, 635.
(40) Moreels, I.; Lambert, K.; Smeets, D.; Muynck, D. D.; Nollet, T.; Martins, J. C.; Vanhaecke, F.; Vantomme, A.; Delerue, C.; Allan, G.; Hens, Z. Size-Dependent Optical Properties of Colloidal PbS Quantum Dots. *ACS Nano* **2009**, *3*, 3023.
(41) Bose, R.; McMillan, J. F.; Gao, J.; Chen, C. J.; Talapin, D. V.; Murray, C. B.; Rickey, K. M.; Wong, C. W. Temperature-Tuning of near-Infrared (1.5-um) Monodisperse Quantum Dot Solids toward Controllable Förster Energy Transfer. *Nano Lett.* **2008**, *8*, 2006.
(42) Sfeir, M. Y.; Qian, H.; Nobusada, K.; Jin, R. Ultrafast Relaxation Dynamics of Rod-Shaped 25-Atom Gold Nanoclusters. *J. Phys. Chem. C* **2011**, *115*, 6200−6207.
(43) Henry, E. R.; Hofrichter, J. *Methods in Enzymology*; Academic Press Inc.: New York, 1992; Vol. *210*, Chapter 8.
(44) Klimov, V. I.; Ivanov, S. A.; Nanda, J.; Achermann, M.; Bezel, I.; McGuire, J. A.; Piryatinski, A. Single-exciton optical gain in semiconductor nanocrystals. *Nature* **2007**, *447*, 441.
(45) Piryatinski, A.; Ivanov, S. A.; Tretiak, S.; Klimov, V. I. Effect of Quantum and Dielectric Confinement on the Exciton−Exciton Interaction Energy in Type-II Core/Shell Semiconductor Nanocrystals. *Nano Lett.* **2007**, *7*, 108.
(46) Efros, A. L.; Rodina, A. V. Confined excitons, trions, and biexcitons in semiconductor microcrystals. *Solid State Commun.* **1989**, *72*, 645.
(47) Kambhampati, P. Unraveling the Structure and Dynamics of Excitons in Semiconductor Quantum Dots. *Acc. Chem. Res.* **2011**, *44* (1), 1−13.